AIAA SciTech Forum
8-12 January 2024, Orlando, FL
AIAA SCITECH 2024 Forum

10.2514/6.2024-2040

On-Orbit Dynamic Thermal Modeling of Large Deployable Mesh Reflectors

N. Tan* and D. Woo†
Lawrence Technological University, Southfield, MI, 48075

K. Zhou‡
The Hong Kong Polytechnic University, Hong Kong, China

C. Kazoleas§, J. Zhang ¶ and S. Yuan‖
The University of Alabama, Tuscaloosa, AL, 35487

Large deployable mesh reflectors are crucial in space applications due to their lightweight and efficient storage characteristics. However, achieving high surface accuracy and managing the significant thermal effects experienced during on-orbit operations remain challenges in deployable mesh reflector design. This paper presents an innovative dynamic thermal modeling methodology for large deployable mesh reflectors, effectively addressing these obstacles. The proposed method considers a comprehensive set of radiation factors including solar, Earth, Albedo, and reflector emissions. This allows for a detailed analysis of dynamic thermal behavior of the reflector, thereby accurately capturing the impact of thermal strains of cable members on surface accuracy. Simulations of a 101-node center-feed parabolic reflecting surface of a deployable mesh reflector indicate that the proposed method can reveal non-uniform temperature distributions, unlike traditional methods that presuppose uniformity. Additionally, the proposed method has proven effective in accurately predicting the root-mean-square error increase of the reflector, typically unobserved in traditional thermal modeling techniques.

I. Nomenclature

Q^{α}	=	the absorbed solar energy by the reflecting surface
α^{S}	=	fraction of straight solar energy absorbed by the reflecting surface
S	=	the solar flux
β	=	angle between the normal vector of mesh facets and the direction of the sun
Q_{Albedo}	=	albedo radiation flux of earth
γ^{a}	=	the albedo constant
$Q_{i,DMR}$	=	radiation emissions of the i-th isothermal unit
ϵ_i	=	emissivity of each isothermal unit of the reflecting surface
σ	=	the Stefan-Boltzmann constant
s_i	=	radiating area of the i-th unit
$T_i^4(t)$	=	temperature of the isothermal unit at time t
k	=	thermal conductivity
q	=	rate of heat flux radiation
ρ	=	density of the reflecting surface material
c	=	specific heat of the material
ϵ_t	=	thermal strain of cable members
L_0^t	=	undeformed length of a member under thermal strain

*Graduate Student, A. Leon Linton Department of Mechanical, Robotics and Industrial Engineering, Student Member of AIAA.
†Assistant Professor, Department of Civil And Architectural Engineering.
‡Assistant Professor, Department of Civil and Environmental Engineering.
§Graduate Student, Department of Aerospace Engineering and Mechanics
¶Graduate Student, Department of Aerospace Engineering and Mechanics
‖Assistant Professor, Department of Aerospace Engineering and Mechanics, Member of AIAA, sichen.yuan@ua.edu

L_0 = undeformed length of a cable member at room temperature
φ_i = Square of the deviation between the i-th facet and desired working surface
A_i = area of the i-th facet of the DMR mesh
μ = normal distance of the facet
(τ, υ) = local coordinate system on the i-th facet plane
δ_{rms-d} = direct Root Mean Square error
A_{mesh} = total area of all facets of the mesh geometry of the reflecting surface

II. Introduction

Over the past several decades, large deployable mesh reflectors (DMRs) have garnered significant research interest due to their lightweight and high storage efficiency in space applications [1–3]. The DMR was first introduced by Miura [4] as a concept of tension truss antenna, wherein a three-dimensional integrated cable lattice system is utilized to form a parabolic reflecting surface. The tension truss antenna is composed of a triangular-faceted cable truss, an RF reflector surface, and a supporting structure that offers both support and pretension to the cable lattice. This concept was later applied in development of the AstroMesh space antenna system [5], shown in Fig. 1, featuring a pair of ring-stiffened geodesic truss domes deployed by a single cable. This design resulted in reduced mass, stowed volume, surface distortion, cost, and program schedule duration compared to other mesh reflectors.

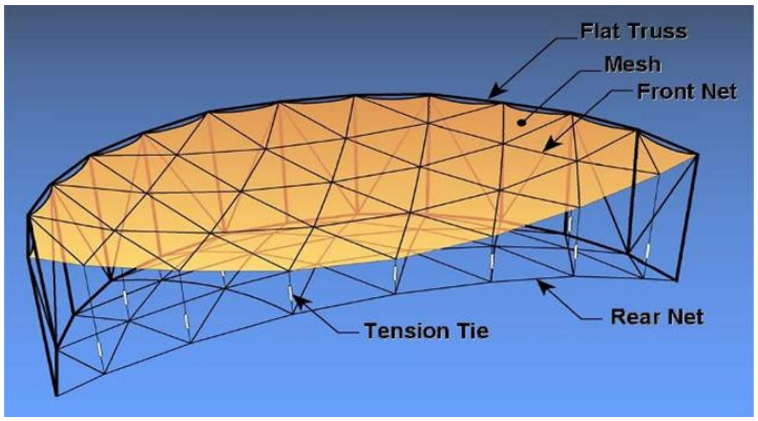

Fig. 1 The AstroMesh space antenna system with deployed working surface.

The reflecting surface accuracy and overall performance of a DMR is determined by its geometric configuration. Thus, the generation of accurate mesh geometry and the accuracy evaluation for the reflecting surface are two important tasks in DMR design. For generation of mesh geometry, Shi et al. [6] presented a new optimal geometry mesh design method for large DMRs. In this method, the mesh geometry of a DMR is generated by pseudo-geodesic curves to ensure high surface accuracy, uniform member lengths, and minimized total member lengths. This method was further improved by Yuan et al. [7] who introduced the projecting surface method (PSM). By intentionally placing nodes off the working surface, the PSM addressed surface errors resulting from node placement on the desired working surface, and optimized mesh geometry to achieve higher surface accuracy for the reflector. For accuracy evaluation of the reflecting surface, the root-mean-square (RMS) error, which measures deviation of the mesh geometry from the desired working surface, is usually used [8]. In general, there are three commonly used methods of calculating the RMS error: nodal deviation RMS error [9], best-fit surface RMS error [10], and direct RMS error [11]. It is important to note that the nodal deviation RMS error and the best-fit surface RMS error do not measure the actual deviation of the mesh geometry from the desired working surface. When stringent requirements for high reflecting surface accuracy in DMR design are imposed or when nodes of a mesh geometry are positioned off the desired working surface as mentioned previously, the direct RMS error becomes necessary for a more precise evaluation.

During its on-orbit mission, a DMR undergoes significant temperature fluctuations as it transitions in and out of the Earth's shadow. These thermal effects can lead to strain in the cable members of the reflector due to thermal expansion, potentially resulting in notable shape distortion. This is attributed to the high susceptibility of cable members to lateral load changes, given the lack of shear and bending rigidity [12]. Such a situation inevitably reduces surface accuracy

and degrades the reflector's RF performance. To address the challenges presented by thermal effects during the design and operation of a DMR, various strategies have been employed. The influence of thermal strains on surface accuracy was first investigated by Hedgepeth [13] from a static point of view, while characterizing the effect by the average temperature change of the reflector. The dynamic thermal effects were assumed to be no more than twice as much of the static effects. Two sources of thermal gradient, temperature differences in structural members due to different angles of solar radiation, and between two faces of the tetrahedral truss due to shading on one face by the other, were also studied. Tang et al.[14] analyzed RMS errors of DMRs by considering the thermal strains as randomly distributed member length errors. Yang et al.[15] treated the thermal strains as a periodic effect, while assuming uniform temperature distribution. Nie et al.[16] analyzed the on-orbit thermal effects of DMRs. The thermal model of the entire reflector, including the cable networks and the supporting ring truss, was established under the non-uniform temperature distribution.

In this study, a novel method for the dynamic thermal modeling of large DMRs has been developed. In this method, not only the solar radiation flux, but also the Earth radiation flux, Albedo radiation flux of Earth and radiation emissions of the reflectors are integrated in the dynamic thermal model so developed. This integrated consideration facilitates an in-depth study of the dynamic thermal behavior and temperature variations among the reflector's cable members, thus accurately capturing the impact of thermal effects on surface accuracy. Unlike traditional thermal modeling methods that presuppose a uniform temperature distribution, the proposed method can uncover non-uniform temperature distributions among the cable members of the reflector. The efficacy of the proposed method is further confirmed through an evaluation of surface accuracy of the DMR; this method is capable of predicting RMS error reductions typically overlooked by traditional thermal modeling techniques.

III. Problem Statement

Large DMRs are incorporated into satellite communication systems alongside other components such as amplifiers, transmitters, and receivers [17]. The functionality of the reflector is elucidated by using a geostationary satellite, whose orbit is presented in Fig. 2. Note that at locations 1, 2, and 3 in Fig. 2, the reflector is subjected to solar radiation, Earth infrared radiation, Earth Albedo radiation. At location 4 of Fig. 2, the reflector is only subjected to Earth infrared radiation. In addition, the DMR has its own radiation emissions during the whole orbital period [18]. A geostationary satellite orbits Earth with a period of 86400 seconds and a velocity of 3.1 km/s [19]. The orbital altitude is approximately 35,788 km, with a zero-degree inclination and zero eccentricity.

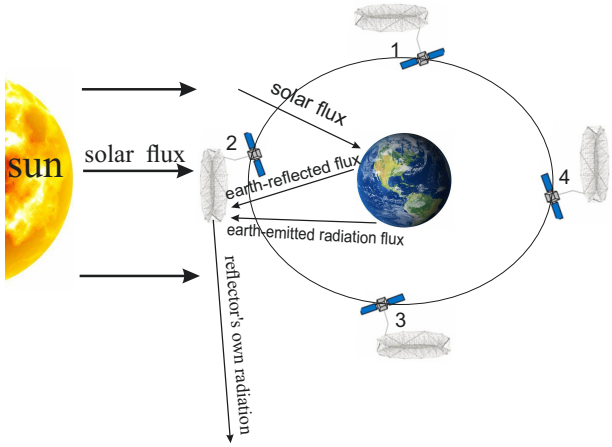

Fig. 2 Heat sources causing major temperature changes of a DMR during the on-orbit mission.

In this paper, the determination of reflecting surface temperature distribution of a DMR is approached under the following assumptions:

1) The reflecting surface of the DMR is treated as a gray body whose surface temperature is changed by heat exchange and balance with its surrounding environment. The influence of minor factors such as heat convection and radiation from satellites is ignored for simplification.
2) The heat exchange between the reflecting surface and its surrounding environment comes from the following four sources: solar radiation flux, Earth infrared radiation flux, Albedo radiation flux of Earth and radiation emissions

of the reflector. Other sources of radiation in the universe are neglected.

3) Comprehensive radiation and heat conduction are considered as the two ways of heat transfer in the dynamic modeling of the reflecting surface.
4) The parabolic reflecting surface is assumed shallow and therefore, is treated as a planar disk in the dynamic thermal modeling.
5) The reflector is fabricated and assembled at room temperature ($21^{\circ}C$)

IV. Analysis of Dominant Radiation Flux

The four important contributors to the radiation flux experienced by the reflecting surface of a DMR: solar radiation flux, Earth infrared radiation flux, Albedo radiation flux from Earth, and radiation emissions from the reflecting surface, are extensively discussed in this section. Understanding the characteristics of these contributions is essential in predicting the dynamic thermal behaviors of the reflecting surface.

A. Solar radiation flux

The total solar irradiance (TSI), which is the amount of solar radiation received at the top of the Earth's atmosphere, has a best estimate of 1361 W/m^2. It is composed of three components, ultraviolet (7%), visible (46%) and infrared radiation (47%). Although some factors such as atmospheric absorption and scattering may cause Earth's atmosphere to receive inconstant solar radiation, the TSI can still be treated as constant according to the measurement results in Ref. [20]. The formula of solar radiation flux to the reflecting surface of a DMR can be derived as:

$$Q^{\alpha} = \alpha^{S} S cos\beta \tag{1}$$

where Q^{α} is the absorptivity, defined as the amount of solar energy absorbed by the reflecting surface; α^{s} is the fraction of straight solar energy absorbed by the reflecting surface; S is the solar flux; and β is the angle between the normal vector of mesh facets and the direction of the sunlight.

B. Earth radiation flux

Earth radiation flux refers to the energy radiated from Earth's surface and atmosphere to space, mainly in the form of infrared radiation. The Stefan-Boltzmann law states that the average radiation emitted from Earth's surface and atmosphere into the space is equivalent to the black-body radiant heat at -20 °C, giving a nominal value for the Earth's radiant flux at 236 W/m^2, with a 16% of tolerance in accuracy [21]. Since the radiation from Earth and that emitted by the reflector are in the same band, the emissivity ϵ of the reflector radiometer can be used to calculate the proportion of the Earth radiation flux received by the reflecting surface, which shall be introduced in Part D of this section.

C. Albedo radiation flux of Earth

Albedo radiation flux refers to the fraction of incoming solar radiation that is reflected back into space by Earth's surface, without being absorbed or transmitted. The Albedo of a surface is contingent upon various factors, including the surface material's color, texture, and composition. Typically, about 30 % of the solar radiation that reaches Earth's atmosphere is reflected back into space with the remaining 70 % absorbed by the surface and atmosphere [22]. As a fraction of the solar constant, Albedo radiation Q_{Albedo} can be expressed by the following equation as:

$$Q_{Albedo} = \gamma^{a} S \tag{2}$$

where γ^{a} is the Albedo constant.

D. Radiation emissions

When the temperature is above absolute zero, the reflecting surface of a DMR radiates energy into space until reaching thermal equilibrium. The emissivity of the reflecting surface, which is the ability of a surface to emit thermal radiation relative to that of a perfect blackbody, needs to be accurately calculated, so as to determine the radiation intensity and spectrum of the reflecting surface. The calculation should incorporate structural geometry and material of the reflecting surface. By dividing the reflecting surface into several isothermal units, the radiation emissions $Q_{i,DMR}$ of a DMR is given as [23]:

$$Q_{i,DMR} = \epsilon_i \sigma s_i T_i^4(t) \tag{3}$$

where ϵ_i is the emissivity of each isothermal unit of the reflecting surface; σ is the Stefan-Boltzmann constant, with the value being $5.67 \times 10^{-8}\ W/m^2 \cdot K^4$; s_i represents the radiating area of the unit; $T_i^4(t)$ denotes the temperature of the isothermal unit at time t.

V. Dynamic Thermal Modeling and Analysis

In this section, a novel method for the dynamic thermal modeling of large DMRs is introduced. By integrating the dominant radiation flux given in the previous section, the heat conduction model of the reflecting surface of the DMR is first developed. The obtained temperature changes of the cable members of the reflector are then transferred to a thermal strain distribution. The corresponding deformed configuration of the reflecting surface is predicted by the dynamic relaxation method. Finally, the surface accuracy of the deformed reflecting surface is evaluated by the direct RMS error. This dynamic thermal modeling approach is particularly useful for preliminary design and active shape control of large DMRs with optimized thermal performance in space environments.

During the on-orbit mission of a DMR, the temperature changes of the cable members on the reflecting surface can be predicted by the principles of Fourier's law and conservation of energy:

$$k\left(\frac{\partial^2 T}{\partial x^2} + \frac{\partial^2 T}{\partial y^2} + \frac{\partial^2 T}{\partial z^2}\right) + q = \rho c \frac{\partial T}{\partial t} \tag{4}$$

where k is the thermal conductivity; x, y, and z are the spatial coordinates in a three-dimensional domain in which heat is transferred; q is the rate of heat flux radiation; ρ is density of the reflecting surface material; and c is specific heat of the material. The thermal strains ϵ_t of the cable members are calculated by substituting the temperatures obtained by Eq. (4) into Eq. (5) [24]:

$$\epsilon_t = \alpha_t \Delta T \tag{5}$$

where α_t is the coefficient of thermal expansion and ΔT is temperature change, given as $\Delta T = T - T_0$, in which T_0 is the room temperature. The undeformed length L_0^t (with no external loads applied) of a member subject to the thermal strain in Eq. (5) is calculated as

$$L_0^t = (1 + \epsilon_t) L_0 \tag{6}$$

where L_0^t represents the undeformed length of a member under thermal strain; L_0 represents the undeformed length of a cable member at room temperature.

The dynamic relaxation method [25] is a numerical technique for the form finding of initial equilibrium configuration (FF-IEC) and the form finding of deformed equilibrium configuration (FF-DEC) of truss-type structures, such as cable-network structures and tensegrity structures [26]. In this paper, the dynamic relaxation method is applied to the FF-DEC of the reflecting surface of a DMR subject to a shape distortion caused by thermal strain. In this method, by considering all the nodes of the reflecting surface as lumped fictitious masses that is connected with fictitious damping, the equilibrium configuration is obtained by numerically solving the virtual system of ordinary differential equations. Due to the existence of fictitious damping, the node will eventually reach the equilibrium position. The dynamic relaxation method was also further developed. "Kinetic damping" was introduced to replace the conventional damping described above [27]. The structure is analyzed by the procedure introduced above with damping coefficient being set to zero. When a local peak in the total kinetic energy of the system is detected, all velocity components are set to zero.

Once the nodal coordinates of the reflecting surface under the thermal strain are obtained, the surface accuracy is evaluated by the direct RMS error [11]. Unlike the nodal deviation RMS error [9] that fails to consider geometry difference between the facet plane and the best-fit surface RMS error [10] that does not measure the real deviation of the mesh geometry from the desired working surface, the direct RMS error measures the area deviation of a DMR mesh geometry from its desired working surface. Therefore, the direct RMS error is a straight-forward and accurate measurement of surface error, and is applicable to both shallow and deep reflecting surface. It also allows the nodes to be placed off the desired working surface (for the purpose of increasing surface accuracy) [7].

Consider a typical triangular facet in Fig. 3, where the desired working surface is also shown. To calculate the direct RMS error, a local coordinate system (τ, υ) is established on the i-th facet plane, where the origin can be any node of the facet. Let $\mu(\tau, \upsilon)$ be the normal distance from a point on the facet plane to the desired working surface. The square of the deviation φ_i between the i-th triangular facet plane and the desired working surface can be calculated by integrating the normal distance square (μ^2) over the entire surface area of the facet:

$$\varphi_i = \iint_{A_i} \mu^2 d\tau d\upsilon \tag{7}$$

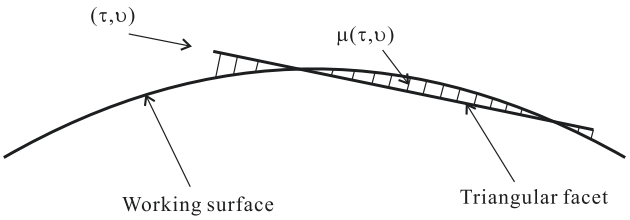

Fig. 3 The desired working surface and a triangular facet for calculation of direct RMS error.

where A_i represents the area of the i-th facet. The direct RMS error δ_{rms-d} of the whole reflecting surface are obtained by the square root of summed and then averaged deviation square:

$$\delta_{rms-d} = \sqrt{\frac{1}{A_{mesh}} \sum_i \varphi_i} \tag{8}$$

Where $A_{mesh} = \sum A_i$ is the total area of all facets of the mesh geometry of the reflecting surface.

VI. Simulation Results

In this section, a DMR with a 101-node center-feed parabolic reflecting surface is investigated for validating the effectiveness of the proposed dynamic thermal modeling method. The DMR is mounted on a geostationary satellite introduced in Section III. The reflecting surface has an aperture diameter (D) of 2 m and a focal ratio (F/D) of 1 (F is the focal length). In dynamic thermal modeling, the reflecting surface of the DMR is treated as a planar disk with a thickness of 10 mm. The material of cable members is Kevlar fiber. The TSI of the reflector is 1361 W/m^2, assuming parallel, direct, and oblique sunlight. Scattered sunlight is ignored. The reflector is also affected by Earth radiation, which has a flux of 239 W/m^2. When the temperature of the reflecting surface rises above absolute zero in space environment, the reflector emits energy into space to achieve thermal equilibrium. Dimensional and material parameters of the cable members of the reflecting surface are given in Table. 1. The proposed method is compared with a traditional method that ignores temperature variation of the reflecting surface of a DMR. In the simulation of the proposed method, the reflecting surface is divided into 10 sections, as shown in Fig. 4. When entering and leaving the Earth's shadow, the sunlight reaches and departs from each section subsequently, which causes corresponding temperature changes in each section.

Table 1 Dimensional and material parameters of the cable members.

Parameter	Values
Young's modulus (Pa)	1.31×10^9
Linear density (g/cm^3)	1.44
thermal expansion coefficient (K^{-1})	13×10^{-6}
Isotropic thermal conductivity ($W \cdot m^{-1}k^{-1}$)	0.04
Specific heat constant pressure ($J \cdot kg^{-1}K^{-1}$)	1380
Emissivity	0.6
diameter (mm)	2

The steady-state dynamic thermal responses of the DMR obtained by the proposed method and the traditional method are presented in Fig.5. One can observe that the proposed method can reveal the significant temperature variation of the reflecting surface during its on-orbit mission. Traditional methodologies often simplify this aspect by assuming a uniform temperature distribution, while the findings in this work suggest an oversimplification.

The superiority of the proposed method is further evidenced in Fig. 6 and Table. 2, where a detailed ten-section temperature heatmap of the DMR at a critical time point (98997 seconds) is presented. This heatmap highlights significant temperature variation. Such detailed thermal profiling is important for enhancing the design and functionality

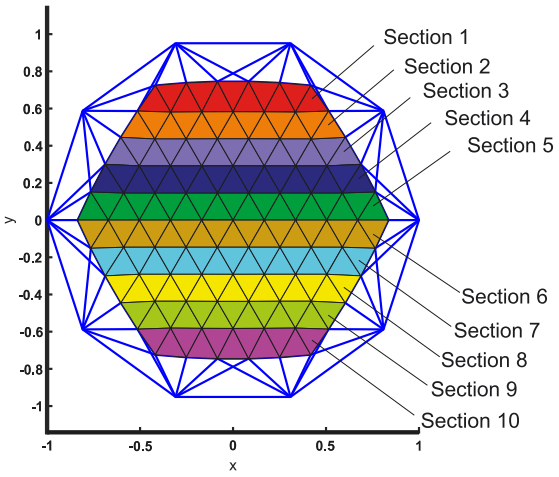

Fig. 4 The 10 divided sections of the reflecting surface.

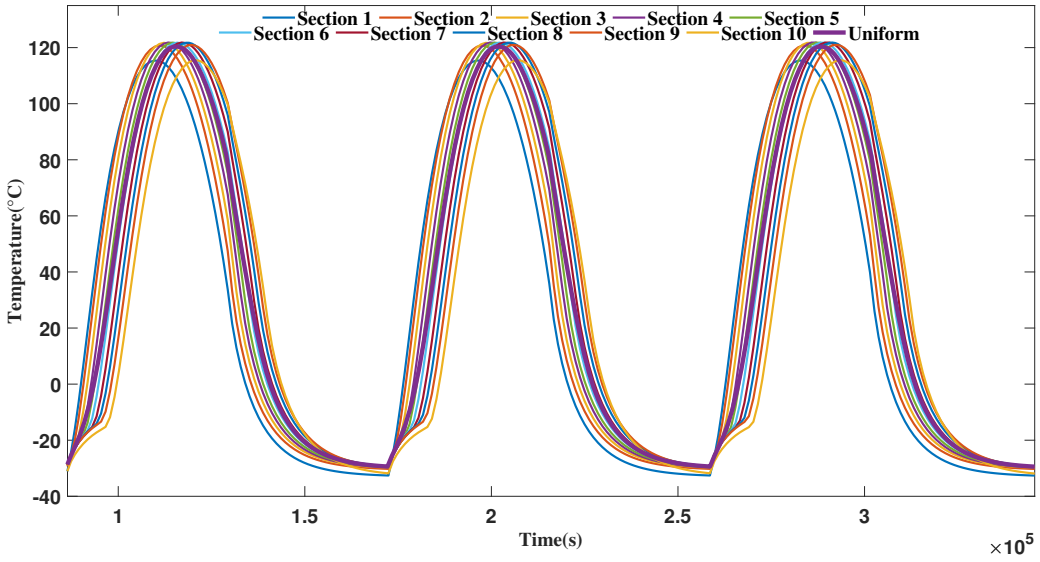

Fig. 5 Temperature Distribution of the Reflecting surface

of DMRs in space missions, offering insights into potential stress points and thermal behavior under varying orbital conditions.

The RMS errors of the DMR obtained by the proposed method and the traditional method are also compared. The undeformed lengths of cable members subjected to the temperature changes given above are first obtained by Eq. (6). The updated nodal positions are then obtained by the dynamic relaxation method introduced in Section V. The RMS errors are finally updated by Eq. (8), where the definition of directed RMS error is used. The simulation results show that the RMS error at the critical time point (98997s) associated with the proposed method is 0.53 mm. The traditional method yields an RMS error of 1.90 mm, which is 358% larger than that obtained by the proposed method. The findings further emphasize the importance of accounting for temperature variations in the thermodynamic modeling of the reflecting surface of a DMR, rather than assuming a uniform temperature distribution. The complex temperature distribution is anticipated to induce substantial thermal strains on the cable members, leading to a further reduction in the reflector's surface accuracy. Consequently, the development of a control algorithm for optimally maintaining the

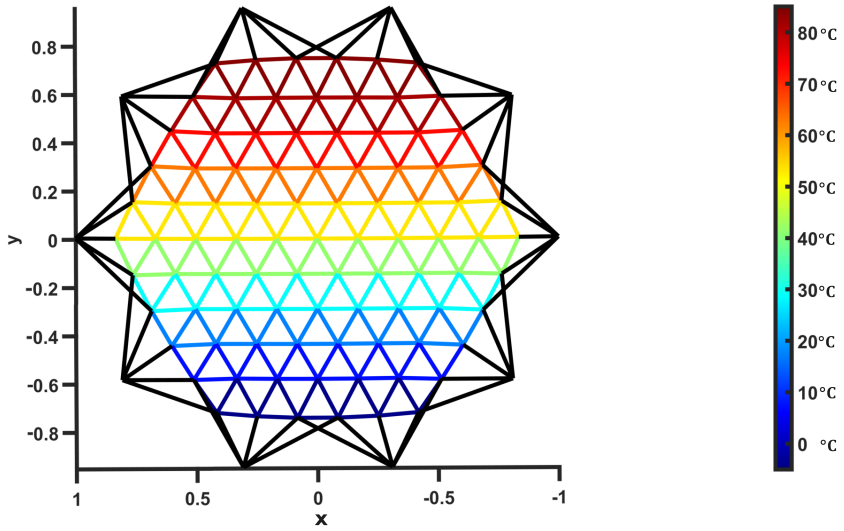

Fig. 6 Ten section geometry's maximum temperature variation heatmap

Table 2 Temperature variation at the critical time point (98997s).

unit	Values (°C)
Section 1	84.097
Section 2	81.338
Section 3	72.744
Section 4	62.702
Section 5	52.924
Section 6	41.512
Section 7	28.638
Section 8	17.257
Section 9	7.0562
Section 10	-4.6152
Uniform	46.11

reflecting surface configuration is deemed necessary and will be the subject of future investigation.

VII. Conclusion

In conclusion, this paper presents a novel method for dynamic thermal modeling of large deployable mesh reflectors in space applications, taking into account the dominant radiation flux experienced by the reflector. The proposed method is demonstrated to be more accurate than traditional approaches, as it captures non-uniform temperature distributions among the cable members of the reflector, which can significantly impact surface accuracy. Simulation results using a reflector with a center-feed parabolic reflecting surface with 101 nodes support the effectiveness of the proposed method. This study highlights the importance of considering temperature variations in dynamic thermal modeling of DMRs, as it affects the reflector's overall performance. The development of a control algorithm to optimally maintain the reflecting surface configuration is suggested for future research. The proposed method offers valuable insights for the design and optimization of DMRs in space environments, paving the way for improved performance and reliability in satellite communication systems.

Acknowledgments

The authors acknowledge support from the US NSF (National Science Foundation) through grant number 2104237.

References

[1] Agrawal, P., Anderson, M., and Card, M., "Preliminary design of large reflectors with flat facets," *IEEE transactions on antennas and propagation*, Vol. 29, No. 4, 1981, pp. 688–694. https://doi.org/10.1109/TAP.1981.1142631.

[2] Yuan, S., Yang, B., and Fang, H., "Self-standing truss with hard-point-enhanced large deployable mesh reflectors," *AIAA Journal*, Vol. 57, No. 11, 2019, pp. 5014–5026. https://doi.org/10.2514/1.J058446.

[3] Nie, R., He, B., Hodges, D. H., and Ma, X., "Integrated form finding method for mesh reflector antennas considering the flexible truss and hinges," *Aerospace Science and Technology*, Vol. 84, 2019, pp. 926–937. https://doi.org/10.1016/j.ast.2018.11.034.

[4] Miura, K., and Miyazaki, Y., "Concept of the tension truss antenna," *AIAA journal*, Vol. 28, No. 6, 1990, pp. 1098–1104. https://doi.org/10.2514/3.25172.

[5] Thomson, M. W., "The Astromesh deployable reflector," *IEEE Antennas and Propagation Society International Symposium. 1999 Digest. Held in conjunction with: USNC/URSI National Radio Science Meeting (Cat. No. 99CH37010)*, Vol. 3, IEEE, 1999, pp. 1516–1519. https://doi.org/10.1109/APS.1999.838231.

[6] Shi, H., Yuan, S., and Yang, B., "New methodology of surface mesh geometry design for deployable mesh reflectors," *Journal of Spacecraft and Rockets*, Vol. 55, No. 2, 2018, pp. 266–281. https://doi.org/10.2514/1.A33867.

[7] Yuan, S., Yang, B., and Fang, H., "The Projecting Surface Method for improvement of surface accuracy of large deployable mesh reflectors," *Acta Astronautica*, Vol. 151, 2018, pp. 678–690. https://doi.org/10.1016/j.actaastro.2018.07.005.

[8] Yuan, S., "Review of root-mean-square error calculation methods for large deployable mesh reflectors," *International Journal of Aerospace Engineering*, Vol. 2022, 2022. https://doi.org/10.1155/2022/5352146.

[9] Li, T., Tang, Y., and Zhang, T., "Surface adjustment method for cable net structures considering measurement uncertainties," *Aerospace Science and Technology*, Vol. 59, 2016, pp. 52–56. https://doi.org/10.1016/j.ast.2016.10.012.

[10] Greene, W. H., "Effects of random member length errors on the accuracy and internal loads of truss antennas," *Journal of Spacecraft and Rockets*, Vol. 22, No. 5, 1985, pp. 554–559. https://doi.org/10.2514/3.25065.

[11] Yuan, S., Yang, B., and Fang, H., "Direct root-mean-square error for surface accuracy evaluation of large deployable mesh reflectors," *AIAA SciTech 2020 Forum*, 2020, p. 0935. https://doi.org/10.2514/6.2020-0935.

[12] Kadlcák, J., *Statics of suspension cable roofs*, CRC Press, 1995.

[13] Hedgepeth, J. M., "Accuracy potentials for large space antenna reflectors with passive structure," *Journal of Spacecraft and Rockets*, Vol. 19, No. 3, 1982, pp. 211–217. https://doi.org/10.2514/3.62239.

[14] Tang, Y., Li, T., Wang, Z., and Deng, H., "Surface accuracy analysis of large deployable antennas," *Acta Astronautica*, Vol. 104, No. 1, 2014, pp. 125–133. https://doi.org/10.1016/j.actaastro.2014.07.029.

[15] Yang, G., Duan, B., Du, J., and Zhang, Y., "Shape pre-adjustment of deployable mesh antennas considering space thermal loads," *Proceedings of the Institution of Mechanical Engineers, Part G: Journal of Aerospace Engineering*, Vol. 232, No. 1, 2018, pp. 143–155. https://doi.org/10.1177/0954410016678432.

[16] Nie, R., He, B., Yan, S., and Ma, X., "Design optimization of mesh antennas for on-orbit thermal effects," *International Journal of Mechanical Sciences*, Vol. 175, 2020, p. 105547. https://doi.org/10.1016/j.ijmecsci.2020.105547.

[17] Imbriale, W. A., and Boccia, L., "Space Antenna Handbook," 2012. https://doi.org/10.1002/9781119945147.

[18] Du, X., Li, M., and Zhao, Y., "The analysis of infrared spectrum of space target," *2010 2nd International Conference on Industrial and Information Systems*, Vol. 2, IEEE, 2010, pp. 525–528. https://doi.org/10.1109/INDUSIS.2010.5565770.

[19] Patel, M. R., *Spacecraft power systems*, CRC press, 2004.

[20] Ball, W. T., Unruh, Y. C., Krivova, N. A., Solanki, S., and Harder, J. W., "Solar irradiance variability: a six-year comparison between SORCE observations and the SATIRE model," *Astronomy & Astrophysics*, Vol. 530, 2011, p. A71. https://doi.org/10.1051/0004-6361/201016189.

[21] Labibian, A., Pourtakdoust, S. H., Alikhani, A., and Fourati, H., "Development of a radiation based heat model for satellite attitude determination," *Aerospace Science and Technology*, Vol. 82, 2018, pp. 479–486. https://doi.org/10.1016/j.ast.2018.09.031.

[22] Kuhn, W. R., and Postawko, S. E., "Solar radiation and the Earth's atmosphere," *The Physics Teacher*, Vol. 26, No. 5, 1988, pp. 266–273. https://doi.org/10.1175/1520-0469(1974)031<0118:APFTAO>2.0.CO;2.

[23] Siegel, R., *Thermal radiation heat transfer*, CRC press, 2001.

[24] Yuan, S., and Jing, W., "Optimal shape adjustment of large high-precision cable network structures," *AIAA Journal*, Vol. 59, No. 4, 2021, pp. 1441–1456. https://doi.org/10.2514/1.J059989.

[25] Barnes, M., "Finding and analysis of tension space structures by dynamic rela fixation," *London: City University*, 1977.

[26] Yuan, S., and Yang, B., "The fixed nodal position method for form finding of high-precision lightweight truss structures," *International Journal of Solids and Structures*, Vol. 161, 2019, pp. 82–95. https://doi.org/10.1016/j.ijsolstr.2018.11.011.

[27] Barnes, M. R., "Form finding and analysis of tension structures by dynamic relaxation," *International journal of space structures*, Vol. 14, No. 2, 1999, pp. 89–104. https://doi.org/10.1260/0266351991494722.